

TIP: Task-Informed Motion Prediction for Intelligent Systems

Xin Huang¹, Guy Rosman², Ashkan Jasour¹,
Stephen G. McGill², John J. Leonard^{1,2}, Brian C. Williams¹

Abstract—Motion prediction is important for intelligent driving systems, providing the future distributions of road agent behaviors and supporting various decision making tasks. Existing motion predictors are often optimized and evaluated via task-agnostic measures based on prediction accuracy. Such measures fail to account for the use of prediction in downstream tasks, and could result in sub-optimal task performance. We propose a task-informed motion prediction framework that jointly reasons about prediction accuracy and task utility, to better support downstream tasks through its predictions. The task utility function does not require the full task information, but rather a specification of the utility of the task, resulting in predictors that serve a wide range of downstream tasks. We demonstrate our framework on two use cases of task utilities, in the context of autonomous driving and parallel autonomy, and show the advantage of task-informed predictors over task-agnostic ones on the Waymo Open Motion dataset.

I. INTRODUCTION

Motion prediction is crucial for intelligent systems. It captures the distribution of future behavior of nearby road agents, and allows intelligent systems to plan and act. Motion predictors often approximate the output distribution via a set of trajectory samples, due to constraints such as the predictor’s computational budget, or the ability of downstream tasks to process the predictions. Traditionally, accuracy-based measures are used to optimize and evaluate the prediction samples, and have proved tremendously useful for reducing and gauging prediction errors. However, they do not account for the relevant downstream task, such as a planner that selects safe and efficient plans by reasoning about the predictions, and a driver assistant system that warns the driver when detecting risky behaviors. These tasks are often safety-critical, as a small error may lead to a catastrophic outcome. Therefore, it is necessary for predictions to better support such tasks, for which they serve as approximate sufficient statistics of nearby road agent behaviors.

Consider a motivating example in Fig. 1, where two predicted samples for an *ado agent*, defined as a nearby road agent of interest, have the same prediction error, in terms of the likelihood given the ground truth future distribution. There are no differences between these two samples when evaluated by task-agnostic accuracy-based metrics. On the other hand, when the prediction is used in a planning system for the *ego agent* that aims to navigate safely with the *ado agent*, one sample may be favored over the other, depending on the ego plan. We illustrate two example scenarios on the

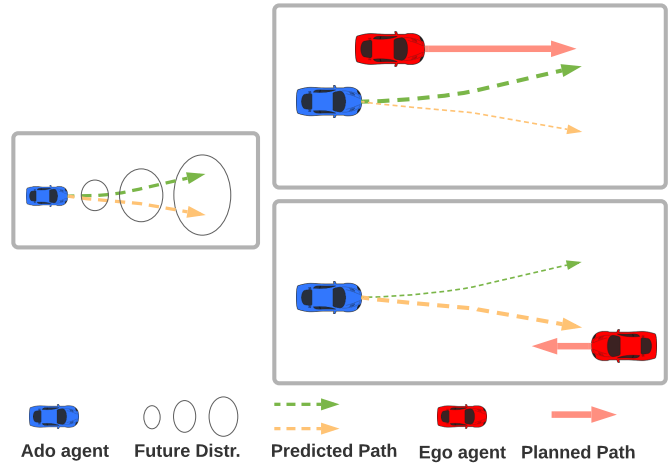


Fig. 1: A motivating example for task-informed prediction, where two samples are predicted for the *ado agent* on the left. The ground truth future distribution is in ellipses. Compared to a task-agnostic predictor that tells no difference between these samples using accuracy-based metrics, a task-informed predictor favors one sample over another, depending on the task information, such as the future plan of the *ego agent*, as illustrated in the two scenarios on the right.

right in Fig. 1. In the top right scenario, the green prediction is more informative as it helps the *ego agent* identify a potential near collision, whereas the orange prediction may lead to an unsafe *ego plan*. The orange prediction is, however, favored in the bottom right scenario, given a different *ego plan*. Therefore, it is crucial to reason about the downstream task when generating predictions.

In this paper, we propose TIP, a Task-Informed motion Prediction framework, where we learn a predictor by jointly optimizing prediction accuracy and the performance of downstream tasks. The training loss leverages a specification of the task, such as its utility function, instead of ignoring the task or requiring the task itself to be co-trained (e.g. optimizing a specific planner with the predictor). This allows the predictors to be used for a variety of tasks within intelligent systems, offering better flexibility and versatility, compared to existing prediction and planning models, which are constrained to a specific task and require that task to be differentiable [1].

Our contributions are as follows: i) We present a task-informed motion prediction framework for intelligent systems that can be used to improve the performance of downstream tasks. Our framework covers a wide range of

¹Computer Science and Artificial Intelligence Laboratory, Massachusetts Institute of Technology, Cambridge, MA 02139, USA
xhuang@csail.mit.edu

²Toyota Research Institute, Cambridge, MA 02139, USA

tasks, thanks to the usage of a versatile task loss function. ii) We show two case studies of our predictor being used in a planning task and a warning task, which are commonly used by state-of-the-art intelligent systems such as autonomous driving and parallel autonomy. iii) We present detailed comparisons to task-agnostic baselines in a realistic large-scale motion prediction dataset and demonstrate that our system helps achieve better task performance.

II. RELATED WORK

A. Motion Prediction

Motion prediction has been studied extensively in the last few years. Learning-based methods demonstrate great success in improving prediction accuracy [2]–[6]. The prediction accuracy is quantified through a few measures, including distance-based metrics such as minimum average displacement error (ADE) and final displacement error (FDE) [2] and distribution-based metrics such as negative log-likelihood (NLL) [7]. However, such accuracy-based metrics do not account for the use of predictions in the downstream task. In other words, predictions with the same accuracy based on minADE or NLL may lead to different outcomes for tasks such as planning, as illustrated in Fig. 1. Therefore, we propose a prediction model that accounts for not only prediction accuracy, but also the utility of the downstream task given the predictions, to allow better integration between predictions and the task.

A concurrent work [8] is proposing task-aware metrics to evaluate motion predictors. It presents a proof-of-concept metric that favors the prediction samples based on the sensitivity to the ego agent’s plan. Results in a synthetic toy dataset show that the presented metric better provides a measure of downstream task performance compared to accuracy-based metrics. We share the same spirit, but push it further to leverage task-specific information to train a motion predictor. This allows us to maximize the value of predictions for downstream tasks, as we demonstrate in realistic driving scenarios. More importantly, by training with a task-informed loss, our predictions cover approximate sufficient statistics [9], [10] of the nearby road agent behaviors for downstream tasks.

B. Prediction for Tasks

Existing works leverage a learned motion predictor to support a variety of tasks, including risk assessment [11], driver safety detection [12], and most commonly, planning for autonomous systems [13]–[19]. They often decouple the optimization of the predictor and the optimization of the task. As a result, the predictor is unaware of its influence on the downstream task and its predictions may not be informative for the downstream task. In this work, we present a more effective predictor that is optimized directly through the utility of the downstream task.

A prior work [12] proposes a multi-task predictor that approximates the utility and its uncertainties of the downstream driver safety detection task, when predicting future driver trajectories. Although the approximated utility statistics are

relevant to the downstream task, the predicted trajectories are learned with a single objective of optimizing the accuracy. On the other hand, our model integrates the task utility into the trajectory prediction directly, allowing the prediction results to better support the task.

Our work is closely related to prediction and planning (P&P) literature [1], which jointly optimizes the prediction module and the planning module. Compared to end-to-end planning models [20]–[22] that generate planning results from raw sensor inputs, P&P, as a more structured approach, provides better interpretability in its decision making process, and achieves better planning performance [1]. One limitation of P&P is that it requires an entire pipeline that includes a differentiable planner so that the planner loss can be back-propagated into the predictor. In contrast, our prediction model only requires the utility function that characterizes the task. As discussed in [8], the utility function is planner-agnostic, allowing the predictor to support a family of planning algorithms, instead of a specific planner as in P&P. Furthermore, a differentiable utility function is usually easier to acquire than a differentiable planner. This makes our model more versatile as it can be applied to non-differentiable planners that are hard to train in a P&P framework and tasks that are more than planners, as we show in our experiments.

Finally, our work relates to several works in perception that reason about the effect of perception uncertainty on downstream tasks [23]–[25].

III. PROBLEM FORMULATION

The prediction system takes input as i) task-specific input information V and ii) observed past trajectories $O = \{\mathbf{o}_t\}_{t=-T_p+1}^0$ over a fixed past horizon T_p , where $\mathbf{o}_t = [o_{1,t}, \dots, o_{N,t}]$ includes continuous positions at time step t for up to N agents. The task input V depends on the specific information from the task, such as an ego planned trajectory, as customary in conditional prediction approaches [26]–[29]. The output is a weighted set of K joint trajectory samples $\mathcal{S} = \{(w^{(k)}, \mathbf{x}^{(k)})\}_{k=1}^K$ for all agents, where $\mathbf{x}^{(k)} = \{\mathbf{x}_t^{(k)}\}_{t=1}^{T_f}$ denotes future trajectory sequences up to a fixed future horizon T_f .

The task-informed prediction aims to allow accurate estimates of task utility for an arbitrary downstream task. We define the task specification as a tuple (\mathcal{I}, u) , where \mathcal{I} is a set of candidate decisions for the task, such as plans of the ego agent, and u is a differentiable utility function mapping a decision $I \in \mathcal{I}$ and the task-informed predictions \mathcal{S} to a scalar.

Finally, we define the task objective to maximize the probability of selecting the optimal decision:

$$R_{task} = \mathbb{P}_I(I_{GT}), \quad (1)$$

where $I_{GT} \in \mathcal{I}$ is the ground truth optimal decision according to u and the ground truth future trajectory $\hat{\mathcal{S}}$, such that $I_{GT} = \arg \max_{I \in \mathcal{I}} u(I, \hat{\mathcal{S}})$, and the probability \mathbb{P}_I depends on the estimated decision utilities given the predictions.

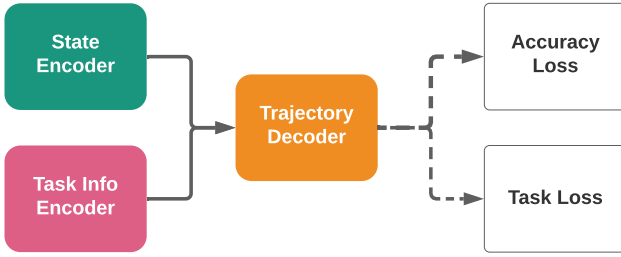


Fig. 2: Diagram of the proposed task-informed prediction model, which includes a state encoder that encodes observed past agent states, a task information encoder that encodes additional task input, and a trajectory decoder that decodes future trajectory predictions. The model is trained through an accuracy loss term that optimizes prediction accuracy and a task loss term that guides the model to favor predictions supporting the downstream task.

IV. APPROACH

Our predictor leverages an encoder-decoder model, as depicted in Fig. 2, following a standard baseline architecture in [30]. The state encoder leverages an LSTM to encode observed agent trajectories into a hidden state. The task information encoder encodes task-specific inputs, such as the future plan of the ego agent, through a separate model. The structure of the task information encoder depends on the input representation, and we defer a detailed description in our experiments. The decoder model takes the concatenated encoded states from both encoders, and predicts a weighted set of K joint trajectory samples \mathcal{S} .

We train the model with the following loss,

$$\mathcal{L} = \mathcal{L}_{acc} + \alpha \mathcal{L}_{task}, \quad (2)$$

where α is used to determine the relative weight between two terms.

The accuracy loss \mathcal{L}_{acc} measures the accuracy of the prediction samples compared to the ground truth future trajectory \hat{S} :

$$\mathcal{L}_{acc} = \sum_{k=1}^K \mathbb{1}(k = \hat{k}) (\log w^{(k)} + \|\mathbf{x}^{(k)} - \hat{S}\|_2), \quad (3)$$

where \hat{k} is the index of the best prediction sample, in terms of $L2$ distance to the ground truth trajectory. This loss is commonly used in multi-model prediction literature [31], [32] to optimize for prediction accuracy while avoiding the mode collapse problem.

The task term \mathcal{L}_{task} minimizes the cross entropy between the probability over decisions and the ground truth optimal decision.

$$\mathcal{L}_{task} = \text{CrossEntropy}(\mathbb{P}_I, I_{GT}), \quad (4)$$

where \mathbb{P}_I comes from the *softmax* over decision utilities [33]:

$$\mathbb{P}(I) = \frac{\exp(u(I))}{\sum_{I' \in \mathcal{I}} \exp(u(I'))}. \quad (5)$$

V. EXPERIMENTS

In this section, we show experimental results in two different tasks to demonstrate the advantage of our proposed task-informed predictor on a naturalistic driving dataset. In each task, we compare our model to task-agnostic baselines and present a representative example to demonstrate its advantage.

A. Dataset

We train and validate our model in the Waymo Open Motion dataset [30]. It is one of the largest motion prediction datasets in terms of the number of scenes, total time, and prediction horizon (e.g. 8 seconds). More specifically, we focus on the pairwise interaction scenarios that are mined to cover interesting interactions between two agents. This allows us to demonstrate the effectiveness of our model in complicated long-term interacting scenarios.

B. Planning for Autonomous System

1) *Task Overview*: In the planning task, the ego agent is controlled by an autonomous system, and its goal is to navigate safely with the presence of an ado agent that is controlled by humans or other intelligent systems.

We assume that the autonomous system is equipped with an arbitrary planner that generates a set of M motion plan candidates $\mathcal{I}_P = \{\tau_1, \dots, \tau_M\}$. The planning utility function is defined as follows:

$$u_P(\tau, \mathcal{S}) = u_{\text{efficiency}}(\tau) + \beta u_{\text{safety}}(\tau, \mathcal{S}), \quad (6)$$

where τ is an ego plan candidate, and $\mathcal{S} = \{(w^{(k)}, x_{\text{ado}}^{(k)})\}_{k=1}^K$ is a weighted set of ado prediction samples, conditioned on the observed trajectory of the ado agent and the ego plan. The efficiency term $u_{\text{efficiency}}$ measures the travelled distance of the ego plan. The safety term u_{safety} measures the expected minimum distance between the ego plan and the ado predictions, computed as follows:

$$u_{\text{safety}}(\tau, \mathcal{S}) = \sum_{k=1}^K w^{(k)} \min_{t=1 \dots T_f} \|\tau_t - x_{\text{ado},t}^{(k)}\|_2. \quad (7)$$

In practice, the improvement of the safety utility diminishes if the agents are far away from each other. Therefore, we upper bound the utility by a safety threshold d_{safe} :

$$u_{\text{safety}}(\tau, \mathcal{S}) = \min(d_{\text{safe}}, \sum_{k=1}^K w^{(k)} \min_{t=1 \dots T_f} \|\tau_t - x_{\text{ado},t}^{(k)}\|_2). \quad (8)$$

2) *Model Details*: The state encoder encodes the observed trajectory points using an MLP with 32 neurons, followed by ReLU and dropout layers with a rate of 0.1. The LSTM has a hidden size of 32 and an output dimension of 32. The task information encoder encodes the planned trajectory of the ego agent, as the task-specific input, through an MLP with 32 neurons, followed by ReLU and dropout layers with a rate of 0.1. The trajectory decoder takes the concatenated encoded states from both encoders, and uses a two-layer MLP with 32 neurons to output the predicted trajectory samples and their

weights. We choose $\alpha = 20$ to keep the two loss magnitudes on the same scale, and $\beta = 5$ to prioritize safe driving. The model is optimized using Adam [34], with a batch size of 32 and a learning rate of 1e-3.

3) *Task Details*: To simulate the planning task, we select the ego agent and the ado agent randomly from the interactive pair in the Waymo data. The ego planner simulates three planned trajectories based on the observed future trajectory of the ego agent. It interpolates and scales the trajectory coordinates by 0.8x, 1.0x, and 1.2x at each time step to simulate conservative driving, normal driving, and aggressive driving. This provides multiple driving options while ensuring the plans are realistic and closely follow the agent intention from data. Examples can be found in Fig. 3.

In order to find the ground truth optimal plan, we also have to simulate the behavior of the ado agent in the future. As we only have access to one ado future trajectory from data, we simulate the other two based on the intelligent driver model (IDM) [35], such that when the ego agent slows down, the ado agent takes advantage and speeds up; when the ego agent moves fast, the ado agent slows down and yields. Examples of reactive ado trajectories can be found in Fig. 3. Simulating realistic ado agent behavior for simulation purposes is a topic of ongoing research [36], and the distribution of the samples is known to affect model training [37]. In our experiments, we follow [19] to use IDM and find it to be effective, as we later show in a qualitative scenario in Sec. V-B.5.

There exist many ways to choose the safety distance threshold d_{safe} , based on the agent size, time-to-collision, and agent velocity. We choose the threshold to be 3.64 meters as the 10% percentile of the pairwise closest distances in the Waymo dataset. This value is smaller than the radius of a regular car with a length of approximately 4.5 meters and a width of approximately 2.0 meters [38], and we defer using a more accurate dynamic threshold as future work.

4) *Quantitative Results*: We compare our proposed model TIP_P with a few baselines. The first one is a Task-Agnostic Predictor (we refer to it as TAP in the rest of the experiments) that uses the same model as ours, but is trained with only the accuracy loss in Eq. (3). Such predictor represents a broad prediction literature that ignores predictions in downstream tasks or decouples prediction and the tasks. This baseline is equivalent to the model proposed in [30], which represents the class of task-agnostic motion predictors that ignore the influence of their predictions on the downstream task. The second one is an end-to-end predictor, E2E_P , that uses the same model as ours, but is trained with only the task loss in Eq. (4).

In addition, we propose two additional models, TIP_{P2} and E2E_{P2} , that are trained for the same planning task but with a different utility function:

$$u_{P2}(\tau, \mathcal{S}) = u_{\text{efficiency}}(\tau_{\text{ado}}) + \beta u_{\text{safety}}(\tau, \mathcal{S}), \quad (9)$$

where τ_{ado} is the simulated trajectory of the ado agent that reacts to the ego plan τ (e.g. as a function of τ). This utility function models an altruistic planner that favors the ado

Model	minADE↓	minFDE↓	AUC-ROC $_P$ ↑	AUC-ROC $_{P2}$ ↑
TAP	3.07	7.26	0.732	0.680
TIP_P	3.08	7.33	0.802	0.620
E2E_P	24.18	45.80	0.798	0.713
TIP_{P2}	3.13	7.30	0.623	0.825
E2E_{P2}	21.91	49.61	0.642	0.842

TABLE I: Comparison between our proposed model and baseline models, in terms of prediction accuracy and task performance, on two tasks P and $P2$. The task-informed predictor trades off little accuracy to much better task performance. It also supports multiple utility functions. The colored cells indicate the results measured by their relevant metrics for the appropriate task.

agent. Such a planner is commonly seen in robotics navigation tasks that try to minimally interfere with humans [15].

We evaluate each model on prediction accuracy and task performance. The prediction accuracy is measured by minADE/minFDE metrics [2], which are standard metrics in motion prediction benchmarks [30], [39]. We measure the task performance through recall and fall-out. Recall measures the percentage of optimal plans that are successfully recognized. Fall-out measures the percentage of false alarms. A perfect decision making system should achieve 100% recall and 0% fall-out. Since our planning system generates soft decisions by assigning probabilities to each candidate plan, we plot the recall and fall-out at various probability thresholds, as receiver operating characteristic (ROC) curve [40], and compute its area under the curve (AUC) score to determine the task performance. AUC-ROC is more statistically consistent and more discriminating than accuracy [41], and is widely adopted in many applications, such as driving [42] and fake news detection [43]. Again, a perfect decision making system should achieve an AUC-ROC score of 1.0. As our planner is dealing with a multi-class decision making problem, we compute the AUC-ROC score using the one-vs-one methodology [44], which is insensitive to data balance [40], [43].

We report two separate AUC-ROC metrics, AUC-ROC $_P$ and AUC-ROC $_{P2}$, depending on which utility function is used to determine the ground truth optimal plan. The results are summarized in Table I, where we color the cell to highlight the model results measured by their relevant metrics. We analyze the results from two aspects as follows.

Trade off accuracy for better task performance While the task-agnostic model (TAP) achieves the best accuracy, our model achieves much better task performance at the cost of little accuracy (c.f. TAP vs. TIP_P , TAP vs. TIP_{P2}). In most cases, the task performance matters more than the prediction accuracy, as the planner interacts directly with the world and a small error may lead to undesirable outcomes. The task performance of our model is comparable to an end-to-end model that is solely optimized towards it (c.f. TIP_P vs E2E_P , TIP_{P2} vs E2E_{P2}), especially in the P task, where TIP_P outperforms E2E_P in terms of AUC-ROC $_P$. On the other hand, end-to-end models produce large prediction errors, making it less suitable if we want to use the predictions

in additional tasks such as time-to-collision detection.

Multiple utility functions We show that our model supports multiple utility functions for the planner, as long as they are differentiable, through results highlighted by the yellow cell. For instance, when training with a different utility function u_{P2} that favors altruistic behavior, our model achieves good task performance on the relevant metric (e.g. TIP_{P2} achieves a high AUC-ROC $_{P2}$ score). This allows the planner to specify an arbitrary differentiable utility function to serve its own need.

5) *Qualitative Results*: In Fig. 3, we present a representative scenario to demonstrate the advantage of our model compared to the task-agnostic baseline. In this scenario, the planner proposes two candidate plans¹ (in magenta) for the ego agent, whose observed trajectory is in red: one *normal* plan that yields to the ado agent, and one *aggressive* plan that speeds up. For each plan, we visualize the simulated future trajectories of the ado agent in cyan and its observed trajectory in blue. In this example, the normal plan has a higher utility function than the aggressive plan, as the latter leads to a near collision, despite that it travels further.

The predictions (in olive) of our predictor and the baseline are visualized in Fig. 3(a) and (b), respectively. In Fig. 3(b), the task-agnostic predictor TAP generates predictions that indicate near collisions for both plans, which lead to a higher utility for the aggressive plan as it travels further. In contrast, in Fig. 3(a), our predictor TIP_P generates predictions that help better approximate the utility for each plan – the normal plan has a higher utility as no near collision is detected, and the aggressive plan has a lower utility due to a near collision indicated by the predictions. As a result, TIP_P helps find the correct decision to choose the normal plan.

C. Warning for Parallel Autonomy

1) *Task Overview*: A pre-collision warning system is widely adopted in parallel autonomy (or shared autonomy), which is a vehicle shared-control framework [12], [45], [46] that monitors driver actions and warns before an unsafe event could happen. The warning system differs from the planning system in a few ways. First, it requires a joint predictor for both ego agent and ado agent, as the ego agent is controlled by a driver and the future path is unknown to the predictor. This requires predicting the joint behavior in the future and determines if a near collision is likely. Second, it provides no task-specific input to the predictor, as it only sends a warning to the driver and does not induce any actual interactions with the world.

The warning system is a binary decision making system that chooses an action from $\mathcal{I}_W = \{\text{warn}, \neg\text{warn}\}$. The utility of a warning action is equivalent to the likelihood of near collision between the ado agent and the ego agent. To compute the near collision likelihood, we follow the two-step procedure given the joint prediction samples $\mathcal{S} = \{(w^{(k)}, x_{\text{ego}}^{(k)}, x_{\text{ado}}^{(k)})\}_{k=1}^K$ for the ego agent and the ado agent. First, the system computes the collision score $r^{(k)} \in \{0, 1\}$

¹We omit the conservative plan in the discussion for the sake of simplicity.

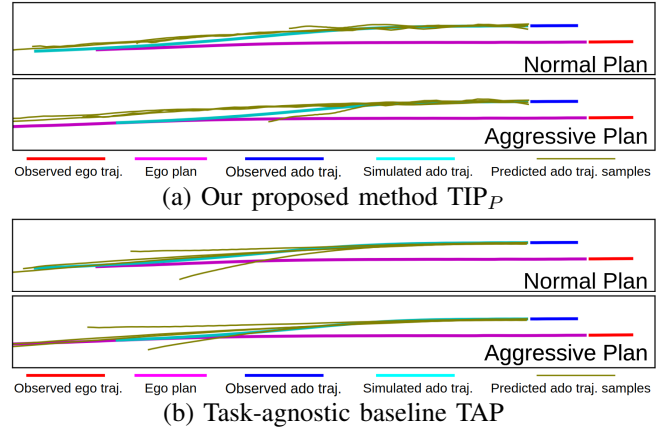


Fig. 3: Predictions from TIP_P (a) and TAP (b) in a representative example, where the aggressive plan has a lower utility than the normal plan, as it leads to a near collision with the ado agent. TIP_P generates predictions, which indicate a near collision for the aggressive plan and no collisions for the normal plan, to help the planner find the correct normal plan. TAP generates predictions that indicate higher utility for the aggressive plan, leading to the wrong decision.

as a Boolean value for each trajectory sample.

$$r^{(k)} = \left(\min_{t=1 \dots T_f} \|x_{\text{ego},t}^{(k)} - x_{\text{ado},t}^{(k)}\|_2 < d_{\text{warn}} \right), \quad (10)$$

where d_{warn} is the minimum safety distance threshold allowed. The collision score is 1 if the closest distance between two agents is smaller than this threshold, and 0 otherwise.

Next, we compute the overall collision likelihood by taking the expected collision score r as the weighted sum of individual warning scores:

$$u_W(\text{warn}) = r = \sum_{k=1}^K w^{(k)} r^{(k)}. \quad (11)$$

Intuitively, the utility of $\neg\text{warn}$ is the likelihood of no near collision, e.g. $u_W(\neg\text{warn}) = 1 - u_W(\text{warn})$.

To compute the ground truth optimal decision, we compute the likelihood of near collision from the observed future trajectories following the same procedure in Eq. (10). Since the observed future trajectories are deterministic, the resulting likelihood is either 0 or 1.

2) *Model Details*: The task-informed predictor model for the warning task leverages the same structure as described in Sec. V-B.2, except that it does not include a task information encoder (e.g. the predictions are conditioned only on past observations). In addition, the utility defined in Eq. (10) is not differentiable due to the Boolean comparison operation. So we utilize a soft warning score using the sigmoid function:

$$r^{(k)} = \text{sigmoid}(d_{\text{warn}} - \min_{t=1 \dots T_f} \|x_{\text{ego},t}^{(k)} - x_{\text{ado},t}^{(k)}\|_2). \quad (12)$$

The soft score is close to 1 when the closest distance is smaller than the safety distance threshold, and close to 0 otherwise. We use the same distance threshold of 3.64 meters as in the planning task.

α	minADE \downarrow	minFDE \downarrow	AUC-ROC \uparrow
0	4.00	10.57	0.165
1	4.05	10.68	0.299
5	4.19	10.98	0.449
20	4.65	11.43	0.643
100	5.29	12.01	0.776

TABLE II: Performance of TIP_W as a function of the task loss coefficient α . Task performance significantly improves at the cost of prediction accuracy.

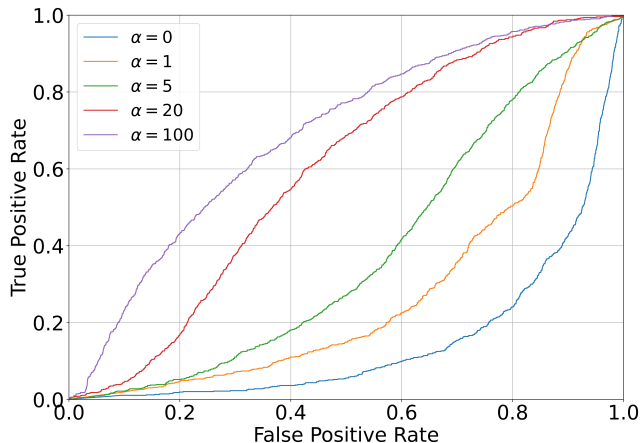


Fig. 4: Visualizations of ROC curves for different values of the task loss coefficient α to train TIP_W . The area under the curve (AUC) of the ROC increases as α increases.

3) *Quantitative Results:* We evaluate the performance of our model using the same accuracy and task metrics as in the planning task. More specifically, we study the model performance under different loss coefficients and numbers of samples to demonstrate its effectiveness.

Effect of the task loss coefficient We perform a study on the trade-off between prediction accuracy and task performance, by tuning the coefficient of the task loss α in Eq. (2). The results are reported in Table II, where the AUC-ROC metrics are computed as the area under the curve from the ROC curves in Fig. 4. When α is 0, the model is equivalent to the Waymo baseline [30] as a task-agnostic predictor (TAP) that is optimized only for accuracy. This model achieves the best minADE/minFDE results. As α increases, the task performance improves at the cost of prediction accuracy. We use $\alpha = 20$ in the rest of the experiments, as it achieves a good balance between accuracy and task performance. In practice, the choice of α depends on the specific requirement of the downstream task and its user.

Approximate sufficient statistics We examine the performance of our model by varying the number of prediction samples. As depicted in Fig. 5, the prediction error (minFDE) decreases as the number of samples increases. On the other hand, the task performance (AUC-ROC) stabilizes at 4 samples. This demonstrates that our model provides predictions with approximate sufficient statistics of the environment for the warning task using only a few samples. The performance

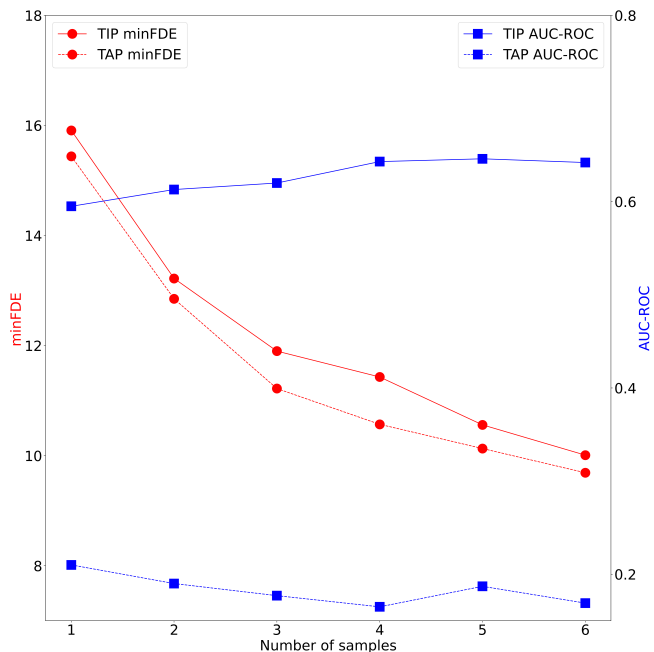


Fig. 5: Performance of TIP_W (solid lines) and the baseline TAP (dashed lines) as a function of the number of prediction samples K . For TIP_W , the prediction accuracy improves as K increases, while the task performance converges at $K = 4$. This indicates that predictions from TIP_W serve as approximate sufficient statistics for the warning task with only 4 samples. Compared to the baseline that is only optimized towards accuracy, TIP_W achieves much better task performance at the cost of little accuracy.

of the task-agnostic baseline TAP is visualized in dashed lines for comparison. The curves show that our proposed model TIP_W achieves much better task performance, by sacrificing little accuracy. In a safety-critical task, improving task performance is crucial, as a mistake in decision making may lead to catastrophic outcomes.

4) *Qualitative Results:* We present a representative warning example in Fig. 6, where the two agents are getting too close according to their observed future trajectories. The closest distance is indicated by the diamond markers. The sample index k is labelled to help identify joint predictions. From the left plot, we see that the task-agnostic baseline fails to identify a likely near collision. Although it predicts a near collision with joint samples #3, they are predicted with a very low probability. On the other hand, our predictor on the right identifies multiple near collision instances, especially through samples #2 that successfully predicts the ado agent is going to cross the ego agent’s path, which matches with what happens in the data. As a result, its predictions indicate a high likelihood of collision and lead to the correct warning decision. This example also shows that in the planning task, it is not required to generate *perfect* predictions, as long as the predictions cover sufficient statistics for the task (e.g. the predictions indicate a collision).

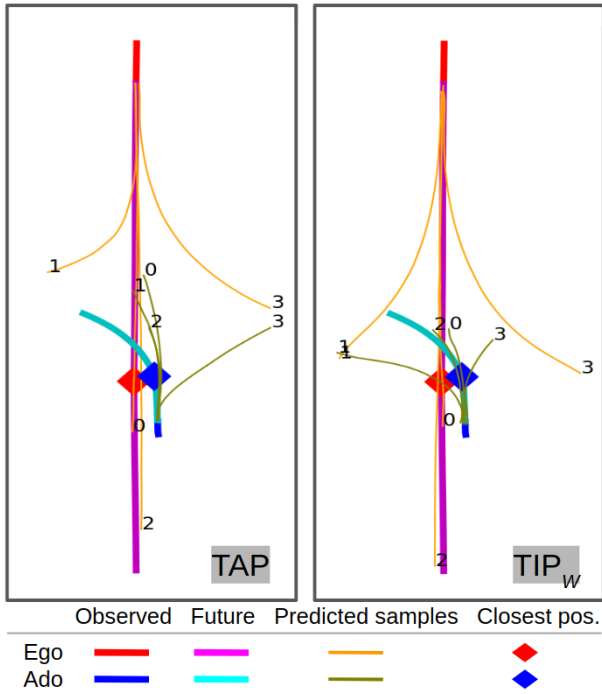


Fig. 6: Comparison between TAP (left) and TIP_W (right) in a warning scenario, where the closest distance between two agents is indicated by the diamond markers. The sample indices are annotated to help associate joint predictions. Our model TIP_W generates predictions that help identify multiple instances of near collisions, especially through joint samples #2 that match with the observed future trajectories.

VI. CONCLUSION

We propose a task-informed motion prediction framework, where predictors are trained to both make accurate predictions and support correct decision making in a downstream task. By leveraging a specification of the task, we allow the predicted samples to provide approximate sufficient statistics of the world for the task, without requiring a full differentiable task for co-training. We demonstrate our predictor in two tasks on the Waymo dataset, and show its advantage compared to task-agnostic and end-to-end baselines.

REFERENCES

- [1] W. Zeng, W. Luo, S. Suo, A. Sadat, B. Yang, S. Casas, and R. Urtasun, "End-to-end interpretable neural motion planner," in *CVPR*, 2019, pp. 8660–8669.
- [2] A. Alahi, K. Goel, V. Ramanathan, A. Robicquet, L. Fei-Fei, and S. Savarese, "Social LSTM: Human trajectory prediction in crowded spaces," in *CVPR*, 2016, pp. 961–971.
- [3] A. Gupta, J. Johnson, L. Fei-Fei, S. Savarese, and A. Alahi, "Social GAN: Socially acceptable trajectories with generative adversarial networks," in *CVPR*, 2018, pp. 2255–2264.
- [4] C. Schöller, V. Aravantinos, F. Lay, and A. Knoll, "What the constant velocity model can teach us about pedestrian motion prediction," *IEEE Robotics and Automation Letters*, vol. 5, no. 2, pp. 1696–1703, 2020.
- [5] J. Gao, C. Sun, H. Zhao, Y. Shen, D. Anguelov, C. Li, and C. Schmid, "VectorNet: Encoding HD maps and agent dynamics from vectorized representation," in *CVPR*, 2020, pp. 11 525–11 533.
- [6] M. Liang, B. Yang, R. Hu, Y. Chen, R. Liao, S. Feng, and R. Urtasun, "Learning lane graph representations for motion forecasting," in *ECCV*. Springer, 2020, pp. 541–556.

- [7] J. Wiest, M. Höffken, U. Kreßel, and K. Dietmayer, "Probabilistic trajectory prediction with gaussian mixture models," in *IV*. IEEE, 2012, pp. 141–146.
- [8] B. Ivanovic and M. Pavone, "Rethinking trajectory forecasting evaluation," *Under review. arXiv preprint arXiv:2107.10297*, 2021.
- [9] B. Jiang, T.-y. Wu, C. Zheng, and W. H. Wong, "Learning summary statistic for approximate bayesian computation via deep neural network," *Statistica Sinica*, pp. 1595–1618, 2017.
- [10] Y. Chen, D. Zhang, M. U. Gutmann, A. Courville, and Z. Zhu, "Neural approximate sufficient statistics for implicit models," in *ICLR*, 2020.
- [11] A. Wang, X. Huang, A. Jasour, and B. Williams, "Fast risk assessment for autonomous vehicles using learned models of agent futures," in *RSS*, 2020.
- [12] X. Huang, S. G. McGill, J. A. DeCastro, L. Fletcher, J. J. Leonard, B. C. Williams, and G. Rosman, "CARPAL: Confidence-aware intent recognition for parallel autonomy," *IEEE Robotics and Automation Letters*, vol. 6, no. 3, pp. 4433–4440, 2021.
- [13] E. Schmerling, K. Leung, W. Vollprecht, and M. Pavone, "Multimodal probabilistic model-based planning for human-robot interaction," in *ICRA*. IEEE, 2018, pp. 3399–3406.
- [14] A. Sadat, M. Ren, A. Pokrovsky, Y.-C. Lin, E. Yumer, and R. Urtasun, "Jointly learnable behavior and trajectory planning for self-driving vehicles," in *IROS*. IEEE, 2019, pp. 3949–3956.
- [15] S. Schaefer, K. Leung, B. Ivanovic, and M. Pavone, "Leveraging neural network gradients within trajectory optimization for proactive human-robot interactions," in *ICRA*, 2021.
- [16] H. Nishimura, B. Ivanovic, A. Gaidon, M. Pavone, and M. Schwager, "Risk-sensitive sequential action control with multi-modal human trajectory forecasting for safe crowd-robot interaction," in *IROS*. IEEE, pp. 11 205–11 212.
- [17] B. Ivanovic, A. Elhafsi, G. Rosman, A. Gaidon, and M. Pavone, "MATS: An interpretable trajectory forecasting representation for planning and control," in *CoRL*, 2021.
- [18] H. Zhu, F. M. Claramunt, B. Brito, and J. Alonso-Mora, "Learning interaction-aware trajectory predictions for decentralized multi-robot motion planning in dynamic environments," *IEEE Robotics and Automation Letters*, vol. 6, no. 2, pp. 2256–2263, 2021.
- [19] S. Casas, A. Sadat, and R. Urtasun, "Mp3: A unified model to map, perceive, predict and plan," in *CVPR*, 2021, pp. 14 403–14 412.
- [20] M. Bojarski, D. Del Testa, D. Dworakowski, B. Firner, B. Flepp, P. Goyal, L. D. Jackel, M. Monfort, U. Muller, J. Zhang *et al.*, "End to end learning for self-driving cars," *arXiv preprint arXiv:1604.07316*, 2016.
- [21] M. Bansal, A. Krizhevsky, and A. Ogale, "ChauffeurNet: Learning to drive by imitating the best and synthesizing the worst," in *RSS*, 2019.
- [22] F. Codevilla, M. Müller, A. López, V. Koltun, and A. Dosovitskiy, "End-to-end driving via conditional imitation learning," in *ICRA*. IEEE, 2018, pp. 4693–4700.
- [23] G. Hager and M. Mintz, "Computational methods for task-directed sensor data fusion and sensor planning," *The International Journal of Robotics Research*, vol. 10, no. 4, pp. 285–313, 1991.
- [24] G. Rosman, C. Choi, M. Dogar, J. W. Fisher, and D. Rus, "Task-specific sensor planning for robotic assembly tasks," in *ICRA*. IEEE, 2018, pp. 2932–2939.
- [25] J. Philion, A. Kar, and S. Fidler, "Learning to evaluate perception models using planner-centric metrics," in *CVPR*, 2020, pp. 14 055–14 064.
- [26] E. Tolstaya, R. Mahjourian, C. Downey, B. Vadarajan, B. Sapp, and D. Anguelov, "Identifying driver interactions via conditional behavior prediction," in *ICRA*. IEEE, 2021.
- [27] J. Ngiam, B. Caine, V. Vasudevan, Z. Zhang, H.-T. L. Chiang, J. Ling, R. Roelofs, A. Bewley, C. Liu, A. Venugopal *et al.*, "Scene transformer: A unified multi-task model for behavior prediction and planning," *arXiv preprint arXiv:2106.08417*, 2021.
- [28] T. Salzmann, B. Ivanovic, P. Chakravarty, and M. Pavone, "Trajectron++: Multi-agent generative trajectory forecasting with heterogeneous data for control," *ECCV*, 2020.
- [29] H. Song, W. Ding, Y. Chen, S. Shen, M. Y. Wang, and Q. Chen, "Pip: Planning-informed trajectory prediction for autonomous driving," in *European Conference on Computer Vision*. Springer, 2020, pp. 598–614.
- [30] S. Ettinger, S. Cheng, B. Caine, C. Liu, H. Zhao, S. Pradhan, Y. Chai, B. Sapp, C. Qi, Y. Zhou *et al.*, "Large scale interactive motion forecasting for autonomous driving: The waymo open motion dataset," *arXiv preprint arXiv:2104.10133*, 2021.

- [31] H. Cui, V. Radosavljevic, F.-C. Chou, T.-H. Lin, T. Nguyen, T.-K. Huang, J. Schneider, and N. Djuric, "Multimodal trajectory predictions for autonomous driving using deep convolutional networks," in *ICRA*. IEEE, 2019, pp. 2090–2096.
- [32] Y. Chai, B. Sapp, M. Bansal, and D. Anguelov, "Multipath: Multiple probabilistic anchor trajectory hypotheses for behavior prediction," in *CoRL*, 2019.
- [33] R. S. Sutton and A. G. Barto, *Reinforcement learning: An introduction*. MIT press, 2018.
- [34] D. P. Kingma and J. Ba, "Adam: A method for stochastic optimization," in *ICLR*, 2015.
- [35] M. Treiber, A. Hennecke, and D. Helbing, "Congested traffic states in empirical observations and microscopic simulations," *Physical review E*, vol. 62, no. 2, p. 1805, 2000.
- [36] H. Caesar, J. Kabzan, K. S. Tan, W. K. Fong, E. Wolff, A. Lang, L. Fletcher, O. Beijbom, and S. Omari, "nuPlan: A closed-loop ml-based planning benchmark for autonomous vehicles," *arXiv preprint arXiv:2106.11810*, 2021.
- [37] C. Finn, S. Levine, and P. Abbeel, "Guided cost learning: Deep inverse optimal control via policy optimization," in *International conference on machine learning*. PMLR, 2016, pp. 49–58.
- [38] N. Niroomand, C. Bach, and M. Elser, "Vehicle dimensions based passenger car classification using fuzzy and non-fuzzy clustering methods," *Transportation Research Record*, p. 03611981211010795, 2021.
- [39] M.-F. Chang, J. Lambert, P. Sangkloy, J. Singh, S. Bak, A. Hartnett, D. Wang, P. Carr, S. Lucey, D. Ramanan *et al.*, "Argoverse: 3D tracking and forecasting with rich maps," in *CVPR*, 2019, pp. 8748–8757.
- [40] T. Fawcett, "An introduction to ROC analysis," *Pattern recognition letters*, vol. 27, no. 8, pp. 861–874, 2006.
- [41] C. X. Ling, J. Huang, H. Zhang *et al.*, "AUC: a statistically consistent and more discriminating measure than accuracy," in *IJCAI*, vol. 3, 2003, pp. 519–524.
- [42] L. Liu, Z. Wang, and S. Qiu, "Driving behavior tracking and recognition based on multisensors data fusion," *IEEE Sensors Journal*, vol. 20, no. 18, pp. 10811–10823, 2020.
- [43] K. Shu, A. Sliva, S. Wang, J. Tang, and H. Liu, "Fake news detection on social media: A data mining perspective," *ACM SIGKDD explorations newsletter*, vol. 19, no. 1, pp. 22–36, 2017.
- [44] D. J. Hand and R. J. Till, "A simple generalisation of the area under the ROC curve for multiple class classification problems," *Machine learning*, vol. 45, no. 2, pp. 171–186, 2001.
- [45] L. Saleh, P. Chevrel, F. Claveau, J.-F. Lafay, and F. Mars, "Shared steering control between a driver and an automation: Stability in the presence of driver behavior uncertainty," *T-ITS*, vol. 14, no. 2, pp. 974–983, 2013.
- [46] W. Schwarting, J. Alonso-Mora, L. Paull, S. Karaman, and D. Rus, "Parallel autonomy in automated vehicles: Safe motion generation with minimal intervention," in *ICRA*. IEEE, 2017, pp. 1928–1935.